

**1 The 11 October 2010 Novaya Zemlya Earthquake:  
2 Implications for Velocity Models and Regional Event  
3 Location**

S. J. Gibbons<sup>1</sup>, G. Antonovskaya<sup>3</sup>, V. Asming<sup>2</sup>, Y. V. Konechnaya<sup>3</sup>, E.  
Kremenetskaya<sup>2</sup>, T. Kværna<sup>1</sup>, J. Schweitzer<sup>1</sup>, and N. V. Vaganova<sup>3</sup>

---

S. J. Gibbons, NORSAR, P.O. Box 53, 2027 Kjeller, Norway. (steven.gibbons@norsar.no)

<sup>1</sup>NORSAR, P.O. Box 53, 2027 Kjeller,  
Norway.

<sup>2</sup>Kola Branch of the Geophysical Survey  
of the Russian Academy of Sciences,  
Apatity, Russian Federation.

<sup>3</sup>Institute of Environmental Problems of  
the North of the Ural Branch of the Russian  
Academy of Sciences, 163002 Arkhangelsk,  
Russian Federation.

4 Characterizing the seismicity of Novaya Zemlya and the surrounding Arc-  
5 tic seas requires accurate event location estimates. Low magnitude events  
6 in this region are currently observed only by a small number of stations in  
7 the European Arctic, with a large azimuthal gap, making the accuracy of  
8 regional velocity models all the more important. Regional traveltime cali-  
9 bration is difficult given the scarcity of sufficiently well constrained events.  
10 On 11 October 2010, a magnitude 4.5 event occurred close to the northern  
11 tip of Novaya Zemlya. This event is significant being the first event in this  
12 region to have been recorded both on the relatively recent regional networks  
13 and arrays, and also teleseismically with good azimuthal coverage. We ex-  
14 amine how well we can constrain the location and origin time using only tele-  
15 seismic phases. Using only first teleseismic P arrivals, we constrain the epi-  
16 center to approximately 76.25N and 64.75E but with no depth resolution.  
17 Clear depth phases, notably on stations in the southern United States, in-  
18 dicate a depth between 9 and 15 km. This independent hypocenter and ori-  
19 gin time estimate allows evaluation of regional phase traveltime prediction  
20 using different models. The predicted Sn traveltime appears to cause the great-  
21 est variability in regional location estimates. The 3-dimensional RSTT (Re-  
22 gional Seismic Travel Times) models provide excellent Pn traveltime esti-  
23 mates for Barents Sea paths but may slightly overestimate Sn traveltimes  
24 from this source region. A modified regional 1-dimensional velocity model  
25 is defined which best predicts Pn and Sn observations at multiple stations

26 up to 15 degrees. The significance of the regional traveltime models for es-  
27 timating location is demonstrated for a low magnitude event on or close to  
28 the northern island of Novaya Zemlya in March 2014, recorded with a sat-  
29 isfactory signal-to-noise ratio at only 4 stations.

## Introduction

30 The Arctic archipelago of Novaya Zemlya, the Kara Sea, and the eastern Barents Sea  
31 are characterized by low seismicity, with fewer than 20 seismic events having been de-  
32 tected in the last 30 years using stations on mainland Europe and on Svalbard. The  
33 small-aperture SPITS and ARCES seismic arrays facilitate a seismic detection threshold  
34 of around magnitude 2 [*Ringdal, 1997; Gibbons et al., 2011*] but, given the poor azimuthal  
35 coverage, the ability to locate low-magnitude events accurately requires accurate travel-  
36 time predictions for regional phase arrivals. Calibrating seismic velocity models requires  
37 reference events of which there are few, if any, with sufficiently low uncertainty in origin  
38 time and location. The era of Soviet nuclear weapons testing on Novaya Zemlya [*Khal-*  
39 *turin et al., 2005*] resulted in many large seismic events for which the source parameters  
40 are well known and which were recorded globally. All of these events however predate the  
41 installation of the highly sensitive SPITS array and most of the network of 3-component  
42 stations. Data from the ARCES array, the KEV station at Kevo in Finland, and a few  
43 stations of the Norwegian National Seismic Network (NNSN) does exist for a few of the  
44 later nuclear tests. A teleseismically recorded event on August 1, 1986, was determined  
45 to be an earthquake due to the observation of clear depth phases [*Marshall et al., 1989*],  
46 but this too predates the regional European Arctic seismic network.

47 Progress has nevertheless been made in constraining regional seismic velocity models.  
48 Using body waves from a number of reasonably well-constrained events, with paths cov-  
49 ering the European Arctic and Barents Sea, *Kremenetskaya et al.* [2001] developed a 1-d  
50 “Barents” velocity model, modified from the IASP91 model [*Kennett and Engdahl, 1991*],

51 with a deeper Moho and higher velocities in the uppermost mantle. This provided a far  
52 better fit to observed seismic traveltimes in the region than the underlying global model  
53 and provided improved seismic location estimates for Ground Truth events. The Barents  
54 model was evaluated and modified [*Schweitzer and Kennett, 2007; Hicks et al., 2004*] to  
55 be based on the more recent AK135 global model [*Kennett et al., 1995*] and with two  
56 alternative 1-dimensional models, *BAREY* and *BAREZ*, differing in the P/S ratio in the  
57 upper mantle, being proposed to model optimally different paths from the Kara Sea to the  
58 Barents Sea. The problem of lacking path coverage for body waves from sufficiently well-  
59 constrained sources can be circumvented by using surface waves for inverting for crustal  
60 and upper mantle velocities. This can be performed for layered models [e.g. *McCowan*  
61 *et al., 1978*] or accommodating lateral variations over extended regions [e.g. *Levshin and*  
62 *Berteussen, 1979*]. In 2003, a project was started to construct a far more detailed model  
63 for the crust and upper mantle below the Barents Sea [*Bungum et al., 2005*], using not  
64 only body wave traveltimes for large seismic events but a large number of datasets such  
65 as deep seismic reflection profiles and surface waves. Products of this collaboration were  
66 the Barents50 model [*Ritzmann et al., 2007*] and BARMOD 3D [*Levshin et al., 2007*].  
67 The latter was based on surface wave tomography of an extended region surrounding the  
68 Barents Sea and indicated anomalously high S-wave velocities in the upper mantle below  
69 the eastern Barents Sea and Kara Sea [see also *Ritzmann and Faleide, 2009*].

70 *Hauser et al. [2011]* consider a probabilistic seismic model for the region comprising many  
71 diverse sets of geophysical data. Rather than specifying a single deterministic velocity at  
72 any given latitude, longitude and depth, they consider probability distributions for seismic

73 velocities over a 3-dimensional grid where the uncertainty at any given node is a function  
74 of the quality of constraints. A probabilistic 3-dimensional velocity model does not result  
75 in a single deterministic event location estimate for a given set of phase arrivals, but  
76 rather a distribution of hypocenters and corresponding event origin times which fit the  
77 distribution of model parameters. The resulting clouds of hypocenters provide the analyst  
78 with a more realistic picture of the uncertainty than the classical error ellipses for which  
79 all uncertainty is assumed to be normally distributed. The primary disadvantage of this  
80 approach is that enormous computational resources are required to calculate the posterior  
81 probability distributions of event hypocenters. The event location procedure described by  
82 *Hauser et al.* [2011] of course is not the only means of incorporating 3-D structure into  
83 event location procedures. The HYPOSAT algorithm and program [*Schweitzer, 2001*] for  
84 example facilitates the use of multiple 1-dimensional velocity models for different groups  
85 of phases and, even using a single global velocity model, relatively unbiased solutions can  
86 be obtained by applying calibrated source specific station corrections [e.g. *Yang et al.*,  
87 2001; *Murphy et al.*, 2005].

88 Significant progress has been made towards fully 3-dimensional tomographic velocity  
89 models [e.g. *Simmons et al.*, 2012, 2015] which have been demonstrated to provide location  
90 estimates for seismic events with greatly reduced uncertainty and bias [*Myers et al.*, 2015].  
91 The Regional Seismic Travel Time (RSTT) software package (see Data and Resources)  
92 was designed to compute rapidly approximate travel times for crustal and upper mantle  
93 phases, accounting for 3-dimensional structure. The techniques for calculating the RSTT  
94 travel times, accounting for lateral variations in seismic wave velocity, are described by

95 *Phillips et al.* [2007]. An initial tomographic study for regional travel times in Eurasia  
96 [described by *Myers et al.*, 2010] formed the basis for RSTT, although the underlying  
97 model is revised continually to incorporate the results from regional tomographic studies.  
98 At the time of writing, the most recent release of RSTT is from April 2014 although all  
99 previous releases of RSTT are still available for download (see Data and Resources) This  
100 allows for a systematic comparison between the performance of subsequent releases.

101 On 11 October 2010, an earthquake exceeding magnitude 4 occurred close to the north-  
102 ern tip of Novaya Zemlya. This was (by a good margin) the largest event on Novaya  
103 Zemlya since the cessation of Soviet nuclear testing [*Gibbons et al.*, 2011] and was well  
104 recorded at regional distances by the arrays and permanent 3-component stations in north-  
105 ern Fennoscandia and on Spitsbergen, in addition to stations of the Arkhangelsk seismic  
106 network [*Morozov and Konechnaya*, 2013] and the network operated by the Kola Regional  
107 Seismological Center (KRSC) on the Kola Peninsula. Fig. 1 displays the beams for the  
108 11 October event recorded at the SPITS and ARCES seismic arrays together with the  
109 locations of the stations within 15 degrees of the epicenter for which Pn and Sn arrival  
110 times could be read with a satisfactory accuracy (Table 1). As is typical for the regional  
111 recordings of Novaya Zemlya events, Pn and Sn are the only visible phases; the Lg phases  
112 which dominate regional recordings along continental paths are blocked on Barents Sea  
113 paths [see *Baumgardt*, 2001].

114 This earthquake is significant since it was recorded at teleseismic distances with ex-  
115 cellent azimuthal coverage. The event is listed in the Reviewed Event Bulletin (REB)  
116 of the International Data Center (IDC) for the Comprehensive Nuclear-Test-Ban Treaty

117 Organization (CTBTO) with the coordinates  $76.2640^{\circ}\text{N}$ ,  $64.7619^{\circ}\text{E}$ , and depth fixed to  
118 the surface. As is clear from Fig. 1, there is a significant discrepancy between the REB  
119 solution (dominated by teleseismic P-phases) and the NORSAR regional reviewed event  
120 location (see Data and Resources section) which is constrained exclusively by P and S  
121 arrivals at regional and intermediate distances up to 25 degrees: all to the West and  
122 South West of the source region. The need to apply station corrections for source-to-  
123 receiver paths from the Barents Sea to stations in Fennoscandia has been documented  
124 [*Yang et al.*, 2001] and it is clear that an event location estimate that does not take ac-  
125 count of 3-dimensional effects will be biased. The bias in the REB solution is likely to  
126 be considerably smaller, although it too is constrained to some degree by regional and  
127 far-regional phases recorded in Fennoscandia. The solution provided by the International  
128 Seismological Center (ISC, see Data and Resources) is indicated in Fig. 1 using an arrow.  
129 This solution is also dominated by teleseismic phases but with regional and far regional  
130 phases to the West and South West, and is close to the REB solution.

131 We seek to provide a more accurate location and origin time for the 11 October event  
132 using only data recorded at teleseismic distances. Since the data at far-regional distances  
133 comes only from a single direction, it is likely that the solution constrained by purely tele-  
134 seismic arrivals will be less strongly biased. With a high confidence hypocenter and origin  
135 time estimate, derived from teleseismic observations with as broad as possible azimuthal  
136 range, we can then assess how well different regional velocity models predict the regional  
137 arrivals given in Table 1. We seek to modify the best of the 1-dimensional models to bet-  
138 ter predict the regional arrivals observed from this event and evaluate how the location



139 estimates for this event using only regional phases vary with the different velocity models.  
140 Finally, we consider a low magnitude event in or close to the northern island of Novaya  
141 Zemlya in March 2014. Without Ground Truth information or teleseismic observations,  
142 we examine the variability of the location estimates possible using the limited observations  
143 at regional distances.

### Locating the 11 October 2010 Novaya Zemlya event Using Teleseismic Data

144 With a magnitude of between 4 and 5, the 11 October event is not observed universally  
145 at the distances for which teleseismic P is anticipated. There is evidence of a signal  
146 at many stations for which the phase onset is too poor to be used for the purposes  
147 of event location. The seismic network of the International Monitoring System (IMS)  
148 for verifying compliance with the Comprehensive Nuclear-Test-Ban Treaty (CTBT) is  
149 typically very effective for the detection and location of earthquakes in remote regions  
150 given the predominance of array stations. A seismic signal which is right at the background  
151 noise level at a single site can be elevated to a clear detection through the stack-and-delay  
152 beamforming operation [e.g. *Schweitzer*, 2014]. [The superiority of the IMS seismic arrays  
153 over the IMS seismic 3-component stations for contributing to built events is demonstrated  
154 by *Kværna and Ringdal*, 2013]. Teleseismic observations from the 11 October event are  
155 displayed in Fig. 2 and the locations of stations where these signals are recorded are  
156 displayed in Fig. 3. We have specifically tried to focus on the distance range from  
157 23 degrees to 80 degrees, avoiding the far regional distance range in which the global  
158 traveltimes are the least reliable [*Myers et al.*, 2015]. This map gives a fairly accurate  
159 detectability map for the event; while some regions of course have very few seismic stations,

160 large regions with few symbols indicate that the event was poorly observed overall. This  
161 is the case for almost all of Canada for example. The most important selection criterion  
162 for stations was that the arrival time of the initial P-phase could be read sufficiently  
163 accurately, although maintaining an a reasonably uniform azimuthal distribution was an  
164 important consideration. For a region such as Europe, with many satisfactory arrival  
165 time readings on array beams, no attempt was made to find signals on complementary  
166 national 3-component stations since an excess of stations from one azimuth would likely  
167 worsen bias in the solution if not addressed by appropriate weighting. For regions with  
168 fewer arrays, all data openly available through the Incorporated Research Institutes for  
169 Seismology (IRIS) Data Management Center (DMC) was obtained in the hope of finding  
170 a few stations with low background noise and/or anomalously high signal-to-noise ratio  
171 (SNR). This included temporary deployments of stations such as the Transportable Array  
172 of the USArray project [FDSN network code TA, *Levander et al.*, 1999] and NECESSArray  
173 in North East China [FDSN network code YP, *Tao et al.*, 2014].

174 Fig. 2 displays a trace for each station that is in some way optimal for picking the  
175 P-wave arrival time. In all cases, a frequency band was selected that optimized the SNR  
176 and, for the array stations, a stack-and-delay beam was formed which optimized the  
177 alignment of traces in the anticipated direction of arrival. While only a single filter band  
178 (1-5 Hz) is displayed, other bands were considered in making the arrival-time picks. The  
179 traces are ordered according to the azimuth from the event location. A small azimuthal  
180 band, between 345 and 355 degrees, contains waveforms which all have a considerably  
181 larger amplitude arrival shortly following the initial P-phase. Most of these stations are

182 temporary sites of the Transportable Array, although this arrival is also observed at the  
183 TXAR array and a few sites of the United States National Seismic Network. These  
184 stations are displayed with white symbols in Fig. 3. Were this later arrival to be a depth  
185 phase, pP - or possibly sP, this would provide a significant constraint on the depth of the  
186 event and therefore also the origin time. Closer inspection of a few other stations, e.g.  
187 PETK, CMAR, NVAR, and DLBC, also indicates a second pulse of energy which could  
188 correspond to a depth phase. Fig. 4 (a) shows VESPA plots [*Davies et al.*, 1971] which  
189 indicate two pulses of coherent energy, separated by approximately 5s, propagating in a  
190 similar direction and recorded at two different seismic arrays at great distance from each  
191 other. In Fig. 4 (b) we demonstrate using three of the Transportable Array stations that  
192 the second phase appears to have a polarity reversal relative to the first phase. The time  
193 delay from positive peak to negative peak is between 4.3s and 4.4s.

194 Fig. 5 shows time residual 1-norms as a function of latitude, longitude, and depth  
195 for the P-wave arrivals displayed in Fig. 2. This is to say that we have placed a trial  
196 hypocenter for our event at every point of a 3-dimensional grid and solved for the origin  
197 time which minimizes the 1-norm of the vector of observed minus predicted traveltime  
198 residuals, where the traveltime is predicted using the AK135 model of *Kennett et al.*  
199 [1995]. The white and the blue stars in Fig. 5 (a) indicate the REB and NORSAR-  
200 reviewed location estimates (see Data and Resources) and the grey lines indicate the great  
201 circle paths to each of the observing stations. The azimuthal coverage is reasonably good  
202 and this is reflected in the high degree of azimuthal symmetry in the residual vector norm  
203 contours. Fig. 5 (b) and (c) display the residual norms from this gridsearch procedure

204 as a function of depth for the lines CD and AB displayed in the map. The HYPOSAT  
205 program allows the depth to be fixed and a best-fit latitude, longitude and origin time to  
206 be found; the small white stars in Fig. 5 (b) and (c) indicate the fixed-depth HYPOSAT  
207 solutions and demonstrate that these are consistent with the results of the independent  
208 gridsearch procedure. We conclude that, using only the initial teleseismic P-wave arrivals,  
209 the epicenter of the earthquake is at approximately  $76.28^{\circ}\text{N}$  and  $64.6^{\circ}\text{E}$  but with the depth  
210 of the event being essentially unconstrained. The trade-off is between the depth and the  
211 origin time, the teleseismic P arrival times being almost equally consistent with an event  
212 at the surface at a time 22:48:26.2 and, for example, an event at depth 50 km at time  
213 22:48:32.9. There is not a significant shift in the epicenter as the depth of the hypocenter  
214 changes. *Bondár et al.* [2004] demonstrate a good correspondence between the epicenter  
215 location accuracy provided by a given teleseismic network and the azimuthal coverage of  
216 the recording stations. For the 66 stations at teleseismic distances used for locating the  
217 October 2010 event, the secondary azimuthal gap is estimated at about 70 degrees (see  
218 figures 2 and 5). From studies of GT5 events, *Bondár et al.* [2004] estimated a median  
219 mislocation of about 7-9 km for events having a secondary azimuthal gap of less than 70  
220 degrees.

221 The depth of an event is of great significance for both structural studies and, for example,  
222 in the context of screening events from potential violations of a nuclear test ban treaty.  
223 In the absence of stations in the immediate vicinity of the epicenter, the depth is typically  
224 determined by detecting evidence of a surface reflection [e.g. *Bonner et al.*, 2002; *Letort*  
225 *et al.*, 2014, 2015]. As with the 1986 Novaya Zemlya/Kara Sea event [*Marshall et al.*, 1989],

226 this event appears to have clear depth phases visible in the waveforms. Ascribing the  
227 identification pP to each of the observed secondary arrivals and solving using HYPOSAT  
228 results in a depth of approximately 13.1 km with an origin time of 22:48:28.2. In order to  
229 assess how sensitive the location is to our identification of these depth phases, a calculation  
230 was also performed in which the phases assumed to be pP were labelled sP. This resulted  
231 in a hypocenter with a depth of 9.8 km and an origin time of 22.48.27.6, a very limited  
232 change in the source parameters.

233 The grid search event location estimation procedure as displayed in Fig. 5 for the  
234 ak135 model was also repeated using traveltimes tables constructed using the 3-dimensional  
235 LLNL-Earth3D model and LLNL-G3Dv3 raytracing software [*Simmons et al.*, 2012]. (The  
236 data and resources section provides a link to the model and software.) The hypocenter  
237 and origin time which minimized the 1-norm traveltimes residual for the 3-D model, using  
238 both teleseismic P and pP depth phases, was  $76.282^{\circ}\text{N}$  and  $64.692^{\circ}\text{E}$ , with depth 11.3km  
239 and origin time 22:48:27.8. This solution is within 2 km in depth and within 5 km laterally  
240 of the estimate obtained using the 1-D ak135 model and the origin time is within 0.4s.  
241 The 1-norm of the traveltimes residual vector was 0.405 for the 3-D calculation compared  
242 with 0.524 for the ak135 calculation, a reduction of approximately 20 percent.

### Evaluating 1-D velocity models to explain regional arrivals

243 With a location estimate and origin time based entirely on teleseismic phase picks, we  
244 evaluate how well commonly applied velocity models match the observed arrival times for  
245 Pn and Sn at the stations displayed in Fig. 1. In addition to the 1-dimensional ak135,  
246 BAREY and BAREZ models, we consider also Pn and Sn times predicted using the 3-

247 dimensional RSTT models. Fig. 6 displays the observed minus predicted travel time  
248 residuals for each of the Pn and Sn arrival time picks listed in Table 1 for velocity mod-  
249 els as displayed, given an origin time of 2010-284:22.48.28.224, a hypocenter 76.2845°N,  
250 64.6505°E, and depth 13.1 km. The RSTT traveltimes were calculated both for the soft-  
251 ware releases in April 2014 (labelled RSTT14) and in October 2010 (labelled RSTT10).

252 The ak135 model overestimates the Pn traveltimes by up to several seconds for the  
253 Barents Sea propagation paths (Fig. 6 a). The BAREY and BAREZ models provide as  
254 expected a better fit for Pn arrivals (the two models having identical P-velocity profiles)  
255 and the Pn predictions from RSTT are very close. RSTT predicts slightly shorter Pn  
256 traveltimes for paths from northern Novaya Zemlya to Svalbard than for northern Novaya  
257 Zemlya to mainland Fennoscandia. The differences are however very small in comparison  
258 with the spread in the data, which is likely to be dominated by uncertainty in the arrival  
259 time picks for these largely emergent onsets. The 2014 RSTT Pn traveltime estimates  
260 from Novaya Zemlya to Svalbard are not significantly different to the estimates from the  
261 2010 RSTT release. For paths from northern Novaya Zemlya to Fennoscandia, the 2014  
262 RSTT release predicts significantly faster traveltimes than the 2010 RSTT release.

263 The predictions for Sn vary greatly with almost 20s separating the slowest arrival pre-  
264 dictions (ak135) from the fastest (BAREZ) for the stations on mainland Europe (Fig. 6  
265 b). The BAREY and BAREZ S-velocity models differ only between 41 km and 410 km  
266 depth with a P:S velocity ratio of 1.72 for the (faster) BAREZ model and 1.77 for the  
267 (slower) BAREY model. The Sn phase arrival picks are as expected more spread than  
268 the Pn picks, although the 7 to 9 second difference between the BAREY and BAREZ

269 predicted traveltimes is significantly greater than the 2 to 3 second variability in the ar-  
270 rival time estimates. Comparing a linear regression of the BAREZ residual points (3-4s  
271 too fast) and a linear regression of the BAREY residual points (5-7s too slow) indicates  
272 that a modification of BAREY/BAREZ with a P:S ratio of 1.74 between 41 and 410 km  
273 depth would likely fit the observations better. We label this velocity model BS174. The  
274 RSTT Sn traveltimes predictions from the 2010 release are better than the ak135 predic-  
275 tions but significantly poorer than either BAREY or BAREZ. The predictions from the  
276 2014 RSTT release are similar to the BAREY model estimates: far more consistent with  
277 the observations than for the 2010 release.

278 While the fit for Pn is far better than for Sn, a 0.5 percent increase in the upper mantle  
279 P-velocity can be demonstrated to reduce the absolute residuals in Fig. 6 a). We call the  
280 velocity model with the S-wave velocity structure of BS174, combined with this marginally  
281 increased P-wave velocity profile, NZ2010. The P and S velocity profiles for BAREY and  
282 BAREZ, together with the modifications, are displayed in Fig. 7 and tabulated in Table  
283 2.

284 Traveltimes residuals as displayed in Fig. 6 were calculated for a large number of alterna-  
285 tive candidate hypocenters and origins which were similarly consistent with the teleseismic  
286 observations. Although small perturbations to the latitude, longitude, depth and time of  
287 the source resulted in small changes to the traveltimes residuals, the patterns displayed in  
288 Fig. 6 appear to hold for all likely source locations and origin times.

289 While we can draw conclusions as to the suitability of velocity models by examining  
290 the residuals as displayed in Fig. 6, the true test is the influence the models have on

291 event location. If we attempt to locate the 11 October event ignoring all stations at  
292 distances greater than 15 degrees, we are left with the arrival time readings provided  
293 in Table 1. Fig. 8 displays location estimates using only these phase arrivals and the  
294 velocity models as indicated together with the teleseismic reference location. That the  
295 NZ2010 model location comes closest to the reference location is not in itself significant;  
296 the modifications to the velocity profiles were chosen specifically to optimize the fit for  
297 exactly these arrivals. What is of greatest interest is the geographical bias resulting from  
298 applying different velocity models when the observing stations all lie within a 90 degree  
299 wide band of azimuth from the event's true location. The faster S-wave velocities in the  
300 BAREZ model pull the preferred location almost 50 km to the East. The slower BAREY  
301 model S-velocities draw the event a similar distance to the West. In the absence of stations  
302 in the wide azimuthal gap, it is the S-wave arrivals that primarily constrain the distance  
303 the event appears to be from the observing stations to the West and South West. Fig. 8  
304 gives an impression of the extent to which the event locations are subject to uncertainty  
305 in the S-wave velocity models. Note that the spread in the event location estimate for  
306 regional stations and different velocity models is over an order of magnitude greater than  
307 the anticipated uncertainty in the event location from the teleseismic observations. A  
308 similar observation was made by *Schweitzer and Kennett* [2007].

### Consequences for Regional Event Location

309 On 4 March 2014 a far smaller event occurred on or close to the northern island of  
310 Novaya Zemlya. With an approximate magnitude of 3, this event is far more typical of  
311 the Novaya Zemlya seismicity which needs to be detected, located, and classified. Signals



312 from this event were only recorded well on a very limited number of stations. The signal  
313 on the SPITS array is by far the best observed, although the recordings on ARCES and  
314 KBS are sufficient for Pn and Sn arrival times to be read with a sufficient accuracy for use  
315 in location procedures. While there are now far more stations than previously in northern  
316 Fennoscandia and on Svalbard, the signal-to-noise ratio for an event of this magnitude  
317 is still too low on most stations for these recordings to be useful. The monitoring at  
318 low magnitudes for the region is still dominated by the SPITS and ARCES arrays and  
319 only the very best of the network 3-component stations. This event is interesting from a  
320 location perspective since it is also observed on the new station ZFI2 on Franz Josef Land  
321 [see *Morozov et al.*, 2015]. Fig. 9 displays traces optimized for the observation of Pn and  
322 Sn at the ZFI2, SPITS, ARCES, and KBS stations. Signals on all other available stations  
323 were deemed to be of too poor quality for use in the location procedure.

324 The March 2014 event is about 300 km further south than the 11 October 2010 event  
325 and, depending upon the significance of the 3-dimensional velocity structure, the per-  
326 formance of the 1-dimensional models may be significantly different to that observed for  
327 the northern tip of Novaya Zemlya. It is important to note that, for this event, we have  
328 no ground truth and no independent seismic observations that can constrain the event  
329 location. The Pn and Sn phase arrival times listed in Table 3 are the only pieces of in-  
330 formation we have to locate the event. For each of the models ak135, BAREY, NZ2010,  
331 and BAREZ, we locate the event using HYPOSAT (depth fixed to the surface) using  
332 two different networks. We consider the ARCES, SPITS, and KBS network which has

333 recorded most of the low magnitude Novaya Zemlya events over the previous two decades,  
334 and then the full set of stations displayed in figures 9 and 10 a).

335 Fig. 10 b) shows the location estimates for the 3- and 4-station configurations using  
336 the models as indicated. The ak135 model places the event at sea. The BAREY and  
337 BAREZ models place the event at the West and East coasts of the northern island of  
338 Novaya Zemlya respectively. The NZ2010 model with its intermediate upper mantle S-  
339 velocity structure places the event on land approximately half way between the East  
340 and West coasts. Numerous attempts were made to locate the events using arrival time  
341 estimates perturbed slightly from the times provided in Table 3 and this was found to  
342 have a negligible result in the location estimates; the S-wave velocity model is far more  
343 significant. The time-residual norms for the ak135 model are significantly higher than for  
344 the other models, although the minimum time residual alone is not sufficient to favor any  
345 one of the BAREY, NZ2010, or BAREZ models over any of the others. If a 1-dimensional  
346 velocity model provides reasonable fidelity over the region to which it is supposed to apply,  
347 then the location estimate made using the 4-station network should not differ greatly from  
348 that made using the 3-station network. While the differences are not large, the solutions  
349 using the NZ2010 model are moved less by the addition of the readings from the ZFI2  
350 station than the solutions resulting from the BAREY or BAREZ models.

351 A grid-search location estimate for the 4 March event using traveltimes calculated from  
352 the 2014 release of RSTT results in inland location estimates essentially co-located with  
353 the location estimates obtained using the BAREY 1-dimensional model.

## Conclusions

354 The ability to locate low magnitude seismic events in the European Arctic requires ex-  
355 cellent models for seismic wave velocities in the crust and upper mantle. This is primarily  
356 because we are only able to monitor from the northernmost part of mainland Europe and  
357 from Svalbard. The  $m_b = 4.5$  earthquake close to the northern tip of Novaya Zemlya  
358 on 11 October 2010, is unique among seismic events in this part of the world as it is,  
359 to date, the only event that has been recorded both on the regional seismic networks of  
360 the European Arctic and globally at teleseismic distances. By careful consideration of  
361 teleseismic signals, we estimate the epicenter to be  $76.28^\circ\text{N}$ ,  $64.65^\circ\text{E}$  with a likely uncer-  
362 tainty of only a few kilometers. Clear depth phases are observed on many stations, but  
363 are strongest on stations in the southern United States. Assuming these phases to be pP  
364 provides a depth estimate of approximately 12 kilometers and a corresponding origin time  
365 of 2010-284:22.48.28.2.

366 Given that this teleseismic location estimate is entirely independent of the many ob-  
367 servations at distances of 20 degrees or less, we can use this hypocenter and origin time  
368 estimate to evaluate velocity models for predicting regional travel times. We have eval-  
369 uated a number of commonly applied 1-dimensional velocity models in addition to the  
370 3-dimensional RSTT software. The BAREY/BAREZ and RSTT models predict the Pn  
371 arrivals at stations within 15 degrees of the epicenter relatively well although it appears  
372 that the traveltimes are slightly overestimated particularly for the paths towards mainland  
373 Europe. There is however a very large spread in the time-residuals for the Sn phases. Most  
374 of the models predict Sn arrivals that are significantly too late, with the exception of the  
375 BAREZ model which slightly underestimates the traveltime. The BAREY and BAREZ

376 models differ only by the P:S velocity ratio in the upper mantle (1.72 for BAREY and  
377 1.77 for BAREZ) and a new 1-dimension model BS174 (identical to BAREY/BAREZ ex-  
378 cept for a 1.74 P:S velocity ratio) reduces the Sn residuals significantly. A second model,  
379 NZ2010, with the same S-velocity profile as BS174, but with a 0.5 percent increase in  
380 P-velocities between 41 and 410 km depth in addition minimizes the Pn time-residuals.  
381 We hope also that the data presented here will be of use in subsequent 3-dimensional  
382 tomographic studies. The scarcity of well-observed events in this region makes the body  
383 wave arrival data of great interest.

384 The increase in the number of stations in the European Arctic in recent years has been of  
385 great benefit in providing many regional observations of the 11 October 2010 earthquake.  
386 The modifications made to the BAREY/BAREZ velocity models were made on the basis  
387 of observing the residuals displayed in Fig. 6. Had we only had three or four stations  
388 with satisfactory regional phases, the confidence in the significance of the time residuals  
389 would have been substantially lower. However, as the March 2014 event demonstrated,  
390 the detection capability for events in the European Arctic at the lowest magnitudes is still  
391 controlled by the SPITS and ARCES seismic arrays and the most sensitive of the closest  
392 3-component stations. (Newly deployed instruments such as the ZFI2 station may have  
393 significance in future years.) We have reason to believe that the Pn traveltimes predicted  
394 by the 1-dimensional BAREY/BAREZ models, and also by the 3-dimensional RSTT  
395 model, perform well for events in this region. The failing of the existing models appears  
396 to be in the Sn traveltime predictions which appear to be the most significant factor in  
397 the location estimate uncertainties. The 2010 release of RSTT appears to overestimate

398 the Sn traveltimes from this region of the European Arctic significantly. The 2014 RSTT  
399 release predicts Sn traveltimes that are comparable to those predicted by the BAREY  
400 model, providing an improvement on the 2010 release but still based on velocity estimates  
401 that are slightly too low. Together with local 1-D models based on, for example, receiver  
402 function studies [e.g. *Morozov et al.*, 2015], we hope that the data presented in this paper  
403 will contribute to a significant improvement in the coming iterations of the 3-dimensional  
404 models for the crust and uppermost mantle.

405 The teleseismic depth phases were significant for providing an independent constraint  
406 on the event depth and, consequently, the origin time. It is important to note that while  
407 there was evidence at many stations for depth phases, they were clearest at a very small  
408 number of stations with most of the best recordings being on temporary deployments.  
409 We would advocate paying greater attention to depth phases, both in applying advanced  
410 techniques for their detection [e.g. *Letort et al.*, 2015], and in searching additional wave-  
411 forms. Events that are well constrained in time and space using teleseismic data may have  
412 a greater role than previously assumed in the calibration of regional velocity models in  
413 the absence of Ground Truth explosion sources. We have also demonstrated that cross-  
414 border collaboration in the sharing and analysis of seismic data has significant benefits in  
415 optimizing the exploitation of the available observations.

## Data and Resources

416 Waveform data from the SPITS and ARCES arrays is available openly from  
417 <http://www.norsardata.no/NDC/data/autodrm.html> (last accessed March 2016).

418 The APA, TER, and BRBB stations are operated by the Kola Regional Seismolog-  
419 ical Center in Apatity, Russia, and the LSK station is operated by the Institute of  
420 Environmental Problems of the North of the Ural Branch of the Russian Academy of  
421 Sciences, in Arkhangelsk, Russia. The HSPB station is operated by the Institute of  
422 Geophysics of the Polish Academy of Sciences, Warszawa, Poland. The stations HOPEN  
423 and HAMF are operated by the University of Bergen, Norway, and are part of the Nor-  
424 wegian National Seismic Network. The stations HEF and KIF are part of the Finnish  
425 National Seismic Network and operated by the University of Helsinki (data available from  
426 [geofon.gfz-potsdam.de/waveform/](http://geofon.gfz-potsdam.de/waveform/), last accessed March 2016). Data from the stations  
427 KEV, KBS, and LVZ are obtained from the Incorporated Research Institutes for Seismol-  
428 ogy Data Management Center at

429 [http://ds.iris.edu/SeismiQuery/by\\_station.html](http://ds.iris.edu/SeismiQuery/by_station.html)

430 (last accessed March 2016) from the IU and II networks.

431 Waveform data from International Monitoring System stations was obtained from the  
432 International Data Center in Vienna, Austria.

433 Waveform data from the Canadian National Seismograph Network (CNSN) was ob-  
434 tained from Natural Resources Canada at

435 [http://www.earthquakescanada.nrcan.gc.ca/stndon/AutoDRM/autodrm\\_req-eng.php](http://www.earthquakescanada.nrcan.gc.ca/stndon/AutoDRM/autodrm_req-eng.php)

436 (last accessed March 2016).

437 All additional waveforms were obtained via the Incorporated Research Institutes for  
438 Seismology Data Management Center at

439 [http://ds.iris.edu/SeismiQuery/by\\_station.html](http://ds.iris.edu/SeismiQuery/by_station.html)

440 (last accessed March 2016). We have utilized data from the networks AK, KN, KR, KZ,  
441 RO, TA, and YP and gratefully acknowledge the operators of these networks for making  
442 the data available.

443 The event locations is displayed are taken from the NORSAR Reviewed Regional Event  
444 Bulletin available at

445 <http://www.norsardata.no/NDC/bulletins/regional/>. The reviewed location of the

446 11 October 2010 event is found on (<http://www.norsardata.no/NDC/bulletins/regional/2010/10/1400>

447 (last accessed March 2016).

448 The LLNL-G3D global 3-dimensional P-wave velocity model and ray-tracing software  
449 is available from

450 <https://missions.llnl.gov/nonproliferation/nuclear-explosion-monitoring/global-3d-seismic-tomography>

451 (last accessed March 2016).

452 The Regional Seismic Travel Time (RSTT) software is available openly from  
453 <http://www.sandia.gov/rstt/> (last accessed March 2016).

454 The seismic bulletin of the International Seismological Center is available from  
455 <http://www.isc.ac.uk/> (last accessed March 2016).

456 **Acknowledgments.** This effort was partly funded by the NORRUSS Project "Seis-  
457 mological monitoring of geophysical processes in the European Arctic", Research Council  
458 of Norway project number 233973/H30 and Russian Fund of Basic Research grant number  
459 14-05-93080.

460 We are grateful to Nathan Simmons and an anonymous reviewer for insightful comments  
461 and recommendations.

462 All maps in this paper are created using GMT software [*Wessel and Smith, 1995*]. We  
463 are grateful to Ulf Baadshaug at NORSAR for technical assistance.



## References

- 464 Baumgardt, D. R., Sedimentary basins and the blockage of Lg wave propagation in the  
465 continents, *Pure appl. geophys.*, *158*, 1207–1250, doi:10.1007/PL00001221, 2001.
- 466 Bondár, I., S. C. Myers, E. R. Engdahl, and E. A. Bergman, Epicentre accuracy based  
467 on seismic network criteria, *Geophysical Journal International*, *156*(3), 483–496, doi:  
468 10.1111/j.1365-246x.2004.02070.x, 2004.
- 469 Bonner, J. L., D. T. Reiter, and R. H. Shumway, Application of a cepstral f statistic  
470 for improved depth estimation, *Bulletin of the Seismological Society of America*, *92*,  
471 1675–1693, doi:10.1785/0120010128, 2002.
- 472 Bungum, H., O. Ritzmann, N. Maercklin, J. I. Faleide, W. D. Mooney, and S. T.  
473 Detweiler, Three-Dimensional Model for the Crust and Upper Mantle in the Bar-  
474 ents Sea Region, *EOS, Transactions American Geophysical Union*, *86*, 160–161, doi:  
475 doi:10.1029/2005EO160003, 2005.
- 476 Davies, D., D. J. Kelly, and J. R. Filson, The VESPA process for the analysis of seismic  
477 signals, *Nature*, *232*, 8–13, 1971.
- 478 Gibbons, S. J., J. Schweitzer, F. Ringdal, T. Kværna, S. Mykkeltveit, and B. Paulsen,  
479 Improvements to Seismic Monitoring of the European Arctic Using Three-Component  
480 Array Processing at SPITS, *Bulletin of the Seismological Society of America*, *101*(6),  
481 2737–2754, doi:10.1785/0120110109, 2011.
- 482 Hauser, J., K. M. Dyer, M. E. Pasyanos, H. Bungum, J. I. Faleide, S. A. Clark, and  
483 J. Schweitzer, A probabilistic seismic model for the European Arctic, *Journal of Geo-  
484 physical Research*, *116*(B1), B01,303+, doi:10.1029/2010jb007889, 2011.

- 485 Hicks, E. C., T. Kværna, S. Mykkeltveit, J. Schweitzer, and F. Ringdal, Travel-times  
486 and Attenuation Relations for Regional Phases in the Barents Sea Region, *Pure appl.*  
487 *geophys.*, *161*, 1–19, 2004.
- 488 Kennett, B. L. N., and E. R. Engdahl, Traveltimes for global earthquake loca-  
489 tion and phase identification, *Geophysical Journal International*, *105*, 429–465, doi:  
490 10.1111/j.1365-246x.1991.tb06724.x, 1991.
- 491 Kennett, B. L. N., E. R. Engdahl, and R. Buland, Constraints on seismic velocities in the  
492 Earth from travel times, *Geophys. J. Int.*, *122*, 108–124, 1995.
- 493 Khalturin, V. I., T. G. Rautian, P. G. Richards, and W. S. Leith, A Review of Nuclear  
494 Testing by the Soviet Union at Novaya Zemlya, 1955-1990, *Science and Global Security*,  
495 *13*, 1–42, doi:10.1080/08929880590961862, 2005.
- 496 Kremenetskaya, E., V. Asming, and F. Ringdal, Seismic Location Calibration of the  
497 European Arctic, *Pure and Applied Geophysics*, *158*, 117–128, doi:10.1007/pl00001151,  
498 2001.
- 499 Kværna, T., and F. Ringdal, Detection Capability of the Seismic Network of the Interna-  
500 tional Monitoring System for the Comprehensive Nuclear-Test-Ban Treaty, *Bulletin of*  
501 *the Seismological Society of America*, *103*, 759–772, doi:10.1785/0120120248, 2013.
- 502 Letort, J., J. Vergoz, J. Guilbert, F. Cotton, O. Sebe, and Y. Cano, Moderate Earthquake  
503 Teleseismic Depth Estimations: New Methods and Use of the Comprehensive Nuclear-  
504 Test-Ban Treaty Organization Network Data, *Bulletin of the Seismological Society of*  
505 *America*, *104*(2), 593–607, doi:10.1785/0120130126, 2014.

- 506 Letort, J., J. Guilbert, F. Cotton, I. Bondár, Y. Cano, and J. Vergoz, A new, improved  
507 and fully automatic method for teleseismic depth estimation of moderate earthquakes  
508 (4.5<mag<5.5): application to the Guerrero subduction zone (Mexico), *Geophysical Jour-  
509 nal International*, 201(3), 1834–1848, doi:10.1093/gji/ggv093, 2015.
- 510 Levander, A., E. D. Humphreys, G. Ekstrom, A. S. Meltzer, and P. M. Shearer, Proposed  
511 project would give unprecedented look under North America, *Eos Trans. AGU*, 80,  
512 245–251, doi:10.1029/99eo00181, 1999.
- 513 Levshin, A., and K. A. Berteussen, Anomalous propagation of surface waves in the Barents  
514 Sea as inferred from NORSAR recordings, *Geophysical Journal International*, 56, 97–  
515 118, doi:10.1111/j.1365-246x.1979.tb04770.x, 1979.
- 516 Levshin, A. L., J. Schweitzer, C. Weidle, N. M. Shapiro, and M. H. Ritzwoller, Surface  
517 wave tomography of the Barents Sea and surrounding regions, *Geophysical Journal  
518 International*, 170(1), 441–459, doi:10.1111/j.1365-246x.2006.03285.x, 2007.
- 519 Marshall, P. D., R. C. Stewart, and R. C. Lilwall, The seismic disturbance on 1986  
520 August 1 near Novaya Zemlya: a source of concern?, *Geophys. J.*, 98, 565–573,  
521 doi:10.1111/j.1365-246X.1989.tb02290.x, 1989.
- 522 McCowan, D. W., P. Glover, and S. S. Alexander, A crust and upper mantle model  
523 for Novaya Zemlya from Rayleigh-wave dispersion data, *Bulletin of the Seismological  
524 Society of America*, 68(6), 1651–1662, 1978.
- 525 Morozov, A. N., and Y. V. Konechnaya, Monitoring of the Arctic region: contribu-  
526 tion of the Arkhangelsk seismic network, *Journal of Seismology*, 17(2), 819–827, doi:  
527 10.1007/s10950-012-9356-x, 2013.

- 528 Morozov, A. N., N. V. Vaganova, Y. V. Konechnaya, and V. E. Asming, New data  
529 about seismicity and crustal velocity structure of the "continent-ocean" transition zone  
530 of the Barents-Kara region in the Arctic, *Journal of Seismology*, 19, 219–230, doi:  
531 10.1007/s10950-014-9462-z, 2015.
- 532 Murphy, J. R., et al., Calibration of International Monitoring System (IMS) Stations in  
533 Central and Eastern Asia for Improved Seismic Event Location, *Bulletin of the Seismo-*  
534 *logical Society of America*, 95(4), 1535–1560, doi:10.1785/0120040087, 2005.
- 535 Myers, S. C., N. A. Simmons, G. Johannesson, and E. Matzel, Improved Regional and  
536 Teleseismic P-Wave Travel-Time Prediction and Event Location Using a Global 3D  
537 Velocity Model, *Bulletin of the Seismological Society of America*, 105(3), 1642–1660,  
538 doi:10.1785/0120140272, 2015.
- 539 Myers, S. C., et al., A Crust and Upper-Mantle Model of Eurasia and North Africa for  
540 Pn Travel-Time Calculation, *Bulletin of the Seismological Society of America*, 100(2),  
541 640–656, doi:10.1785/0120090198, 2010.
- 542 Phillips, W. S., M. L. Begnaud, C. A. Rowe, L. K. Steck, S. C. Myers, M. E. Pasyanos,  
543 and S. Ballard, Accounting for lateral variations of the upper mantle gradient in Pn  
544 tomography studies, *Geophys. Res. Lett.*, 34(14), L14,312+, doi:10.1029/2007gl029338,  
545 2007.
- 546 Ringdal, F., Study of low-magnitude seismic events near the Novaya Zemlya test site, *Bull*  
547 *Seism Soc Am*, 87, 1563–1575, 1997.
- 548 Ritzmann, O., and J. I. Faleide, The crust and mantle lithosphere in the Barents Sea/Kara  
549 Sea region, *Tectonophysics*, 470(1-2), 89–104, doi:10.1016/j.tecto.2008.06.018, 2009.

- 550 Ritzmann, O., N. Maercklin, J. I. Faleide, H. Bungum, W. D. Mooney, and S. T. Detweiler,  
551 A three-dimensional geophysical model of the crust in the Barents Sea region: model  
552 construction and basement characterization, *Geophysical Journal International*, *170*,  
553 417–435, doi:10.1111/j.1365-246x.2007.03337.x, 2007.
- 554 Schweitzer, J., HYPOSAT - An Enhanced Routine to Locate Seismic Events, *Pure and*  
555 *Applied Geophysics*, *158*(1), 277–289, doi:10.1007/pl00001160, 2001.
- 556 Schweitzer, J., Seismometer Arrays, in *Encyclopedia of Earthquake Engineering*, edited  
557 by M. Beer, I. A. Kougioumtzoglou, E. Patelli, and I. S. Au, pp. 1–11, Springer Berlin  
558 Heidelberg, doi:10.1007/978-3-642-36197-5\_191-1, 2014.
- 559 Schweitzer, J., and B. L. N. Kennett, Comparison of Location Procedures: The Kara Sea  
560 Event of 16 August 1997, *Bull. seism. Soc. Am.*, *97*, 389–400, doi:10.1785/0120040017,  
561 2007.
- 562 Simmons, N. A., S. C. Myers, G. Johannesson, and E. Matzel, LLNL-G3Dv3: Global P  
563 wave tomography model for improved regional and teleseismic travel time prediction,  
564 *J. Geophys. Res.*, *117*(B10), B10,302+, doi:10.1029/2012jb009525, 2012.
- 565 Simmons, N. A., S. C. Myers, G. Johannesson, E. Matzel, and S. P. Grand, Evidence for  
566 long-lived subduction of an ancient tectonic plate beneath the southern Indian Ocean,  
567 *Geophys. Res. Lett.*, *42*(21), 2015GL066,237+, doi:10.1002/2015gl066237, 2015.
- 568 Tao, K., F. Niu, J. Ning, Y. J. Chen, S. Grand, H. Kawakatsu, S. Tanaka,  
569 M. Obayashi, and J. Ni, Crustal structure beneath NE China imaged by NECES-  
570 SArray receiver function data, *Earth and Planetary Science Letters*, *398*, 48–57, doi:  
571 10.1016/j.epsl.2014.04.043, 2014.

- 572 Wessel, P., and W. H. F. Smith, New version of the Generic Mapping Tools, *EOS Trans.*  
573 *Am. Geophys. Union*, 76, 329, 1995.
- 574 Yang, X., I. Bondár, K. McLaughlin, and R. North, Source Specific Station Corrections  
575 for Regional Phases at Fennoscandian Stations, *Pure and Applied Geophysics*, 158(1),  
576 35–57, doi:10.1007/pl00001164, 2001.

**Figure 1 caption**

577 Location estimates for the 11 October 2010 Novaya Zemlya event using regional crustal  
578 phases only (NORSAR) and using global IMS stations (REB solution). The ISC location  
579 estimate uses both IMS and non-IMS stations, at both regional and teleseismic distances.  
580 The stations displayed are those within 15 degrees for which satisfactory readings of  
581 both Pn and Sn phases were made. The regional array stations are labelled with circles  
582 and 3-C stations with triangles. The waveform segments shown have a duration of 10  
583 minutes, starting at a time 2010-284:22.48.25. The beams optimized for the Pn phases  
584 use the vertical channels of the arrays and the beams optimized for the Sn phases use the  
585 horizontal channels, rotated to be transverse to the great-circle paths indicated by the  
586 solid black lines. Please see Data and Resources for event location details.

**Figure 2 caption**

587 Waveforms from 66 stations at teleseismic distances centered on the P-phase arrival.  
588 This UT arrival time on 11 October 2010 is given on the trace. Various bandpass filters  
589 are applied to optimize the signal-to-noise Ratio (SNR). The typical band applied is  
590 1-5 Hz although this varies somewhat from station to station. For array stations, an  
591 optimal beam is displayed. Stations obtained from FDSN networks are preceded by the  
592 2 character network code. All stations without a network code are IMS stations. The  
593 signals are ordered according to station azimuth. The secondary phase (interpreted as a  
594 pP depth phase) is visible on many traces, arriving approximately 5s after P, although  
595 these are clearest on the stations between azimuth 345 degrees and 353 degrees.



**Figure 3 caption**

596 Locations of arrays (circles) and 3-component stations (triangles) that recorded tele-  
597 seismic P phases for the 11 October 2010 Novaya Zemlya event with a satisfactory SNR  
598 (see Figure 2). The IMS seismic arrays are labelled. The stations at which the clearest  
599 depth phases are shown are displayed with white symbols.

**Figure 4 caption**

600 Demonstration of presumed depth phases. (a) shows the VESPA procedure [*Davies*  
601 *et al.*, 1971] for two seismic arrays arrays and demonstrates two distinct pulses of en-  
602 ergy, separated by approximately 5s, propagating from the same backazimuth. (b) shows  
603 waveforms from 3 stations of the US Array Transportable Array in the southern United  
604 States for which the amplitude of the presumed depth phase is greater than the ampli-  
605 tude for the first P arrival. Traces have been aligned according to the arrival picks. The  
606 lowermost trace is generated by correlating a tapered multichannel 10 second long tem-  
607 plate (3-channels) with the data stream with the incoming data. A positive peak (the  
608 autocorrelation) is followed almost 5s later by a negative peak.

**Figure 5 caption**

609 1-norm residuals for the teleseismic P-picks displayed in Figure 2 with respect to the  
610 ak135 model for trial hypocenters as a function of (a) latitude and longitude with depth  
611 fixed to the surface, (b) longitude and depth with latitude fixed to 76.28 degrees North,  
612 and (c) latitude and depth with longitude fixed to 64.65 degrees East. For each trial  
613 hypocenter, the origin time is selected which minimizes this 1-norm residual. The grey  
614 lines show the directions to the stations displayed in Figure 3. The small white stars in  
615 panels (b) and (c) indicate HYPOSAT solutions for fixed depth using only teleseismic P.  
616 The indicated stars in panels (b) and (c) indicate the HYPOSAT solution using P and  
617 presumed pP arrivals without an imposed depth constraint.

**Figure 6 caption**

618 Time residuals with respect to the arrival time picks given in Table 1 using different  
619 models using an event origin time of 2010-284:22.48.28.224 and a hypocenter 76.2845°N,  
620 64.6505°E, and depth 13.1 km. The traveltimes computed for the 1-dimensional models  
621 ak135, BAREY and BAREZ are not dependent upon the direction whereas those for the  
622 RSTT model are calculated point to point using the RSTT software.

**Figure 7 caption**

623 Velocity as a function of depth for the ak135, BAREY and BAREZ models together  
624 with NZ2010: the modification to BAREY/BAREZ which appears to give the best fit to  
625 the regional arrival times listed in Table 1 for the purely teleseismic hypocenter and origin  
626 time for the 11 October 2010 event.

**Figure 8 caption**

627 Location estimates for the 11 October 2010 Novaya Zemlya event using regional data  
628 only (14 stations, Pn and Sn readings listed in Table 1), together with the reference  
629 teleseismic location estimate.

**Figure 9 caption**

630 Regional waveforms for stations as indicated for the 4 March 2014 Novaya Zemlya event.  
631 All Pn traces are vertical components only with the ARCES beam formed using  $v_{\text{app}} =$   
632  $9.1(km/s)$  and backazimuth  $54^\circ$  and the SPITS beam formed using  $v_{\text{app}} = 7.4(km/s)$  and  
633 backazimuth  $107^\circ$ . All Sn traces are constructed from transverse rotations of horizontal  
634 components with the ARCES beam formed using  $v_{\text{app}} = 5.1(km/s)$  and backazimuth  $54^\circ$   
635 and the SPITS beam formed using  $v_{\text{app}} = 4.7(km/s)$  and backazimuth  $107^\circ$ . All beams  
636 are bandpass filtered 4-10 Hz.

**Figure 10 caption**

637 (a) Map of regional stations recording the 4 March 2014 Novaya Zemlya event and  
638 (b) event location estimates of the event using different velocity models. The location  
639 estimates obtained using the 2014 release of RSTT are almost identical to those obtained  
640 using the BAREY model.



**Table 1.** Phase picks at regional distances for the 11 October 2010 Novaya Zemlya event.

Station	Latitude	Longitude	Dist	Azi	Pn pick	SNR	Sn pick	SNR
APA	67.603	32.994	12.9	245	22.51.27.95	4.6	22.53.43.01	1.6
ARCES	69.535	25.506	12.6	257	22.51.28.28	28.6	22.53.43.58	4.5
BRBB	78.059	14.219	10.7	303	22.51.02.36	11.2	22.53.00.00	4.0
HAMF	70.642	23.684	12.7	265	22.51.24.92	7.7	22.53.34.26	7.6
HEF	68.406	23.664	14.4	258	22.51.45.12	11.7	22.54.15.33	11.3
HOPEN	76.508	25.011	9.2	291	22.50.39.46	3.0	22.52.14.03	4.6
HSPB	77.002	15.533	10.7	297	22.51.01.50	65.3	22.52.57.90	30.0
KBS	78.926	11.942	10.9	308	22.51.05.17	5.0	22.53.05.34	3.0
KEV	69.755	27.007	12.1	256	22.51.21.90	10.0	22.53.33.42	15.0
KIF	69.043	20.804	14.6	264	22.51.49.31	3.6	22.54.19.66	3.9
LSK	64.879	45.734	13.0	218	22.51.27.35	5.5	22.53.44.56	4.4
LVZ	67.898	34.651	11.9	240	22.51.18.16	4.0	22.53.25.41	8.0
SPITS	78.178	16.370	10.2	303	22.50.56.35	65.0	22.52.49.00	31.2
TER	69.201	35.108	11.1	246	22.51.03.34	10.9	22.52.59.23	6.2

**Table 2.** Specification of P- and S-wave velocities for travelttime prediction in the Barents Sea region. From a depth of 410 km and greater, all models are identical to AK135 [Kennett *et al.*, 1995]. All velocities are specified in km/s and the superscripts identify the appropriate velocity models: BAREY (A), BAREZ (B), BS174 (C), and NZ2010 (D).

Depth (km)	$v_P^{A,B,C}$	$v_P^D$	$v_S^A$	$v_S^{C,D}$	$v_S^B$
0.0	6.200	6.200	3.580	3.580	3.580
16.0	6.200	6.200	3.580	3.580	3.580
16.0	6.700	6.700	3.870	3.870	3.870
41.0	6.700	6.700	3.870	3.870	3.870
41.0	8.100	8.141	4.576	4.655	4.709
70.0	8.225	8.266	4.647	4.727	4.782
210.0	8.260	8.301	4.667	4.747	4.802
210.0	8.350	8.392	4.718	4.799	4.810
410.0	9.030	9.030	4.870	4.870	4.870
410.0	9.360	9.360	5.080	5.080	5.080
460.0	9.528	9.528	5.186	5.186	5.186

**Table 3.** Phase picks for the 4 March 2014, Novaya Zemlya event.

Station	Latitude	Longitude	Dist	Azi	Pn pick	SNR	Sn pick	SNR
ARCES	69.535	25.506	11.0	260	04.45.06.08	2.2	04.47.02.17	5.0
KBS	78.926	11.942	11.0	314	04.45.06.36	1.6	04.47.04.26	4.1
SPITS	78.178	16.370	10.2	310	04.44.55.53	7.5	04.46.42.98	4.6
ZFI2	80.809	47.655	6.7	346	04.44.08.32	3.9	04.45.17.20	3.5

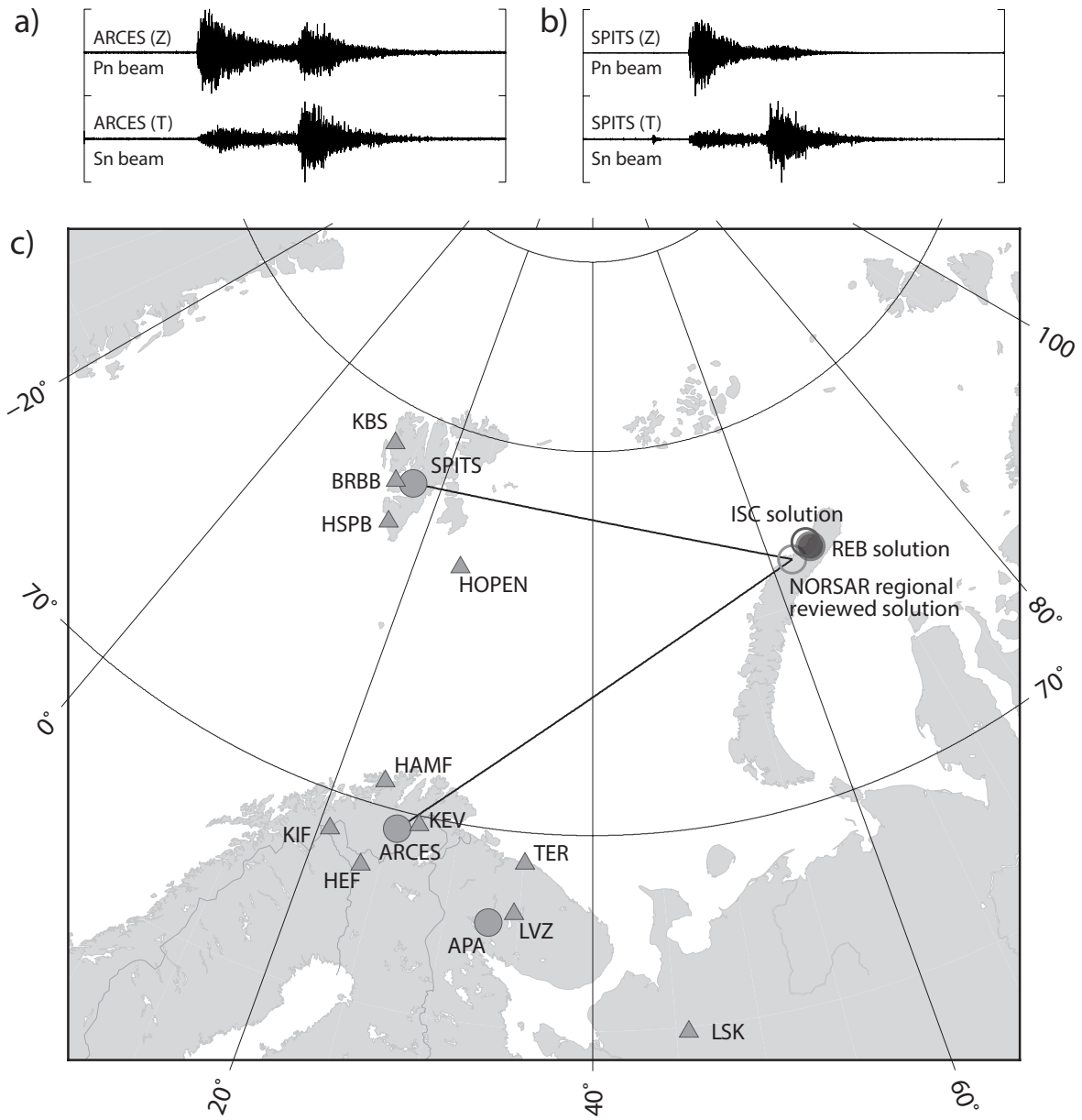


Figure 1. Figure 1 caption.

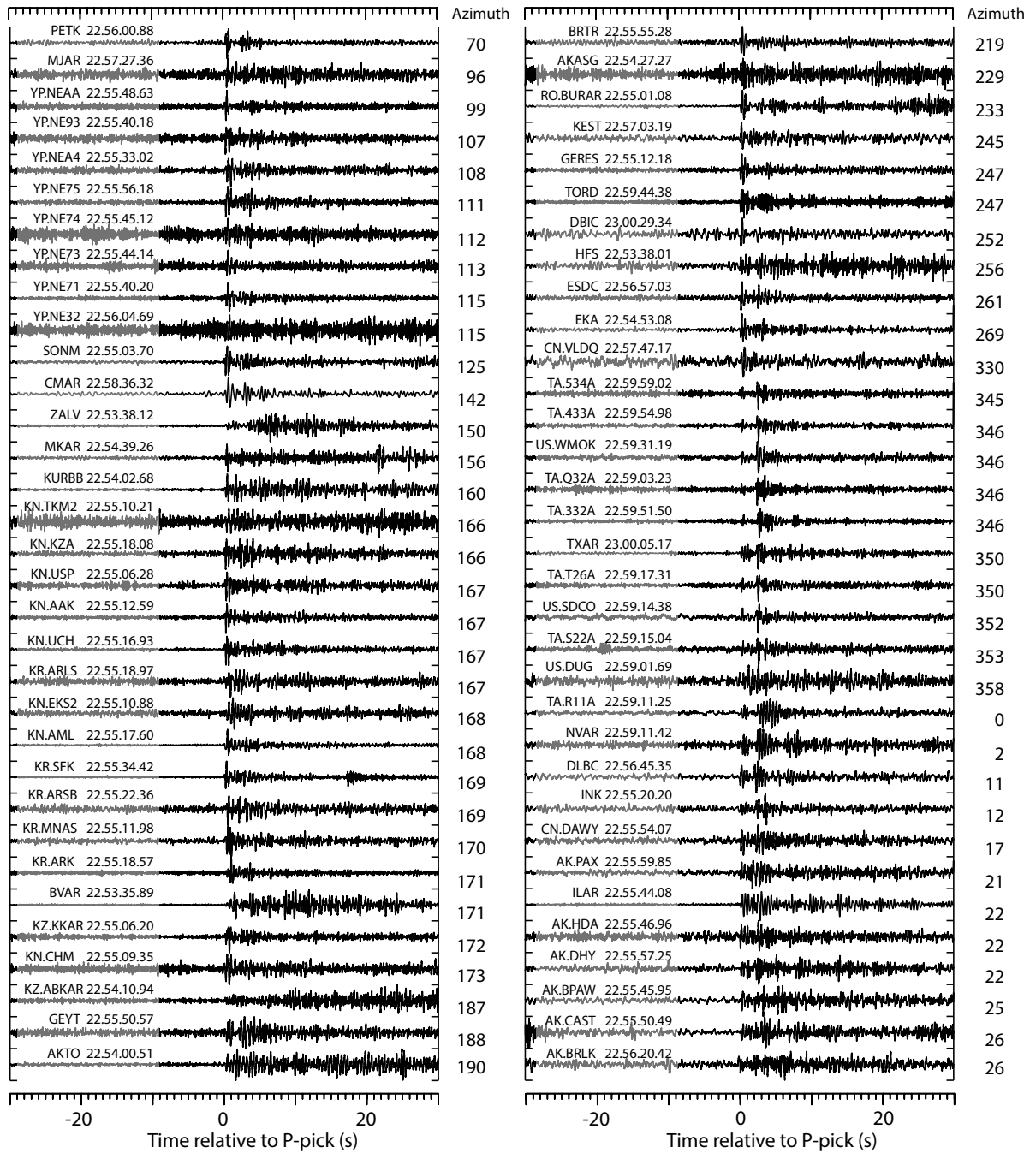


Figure 2. Figure 2 caption.



Figure 3. Figure 3 caption.

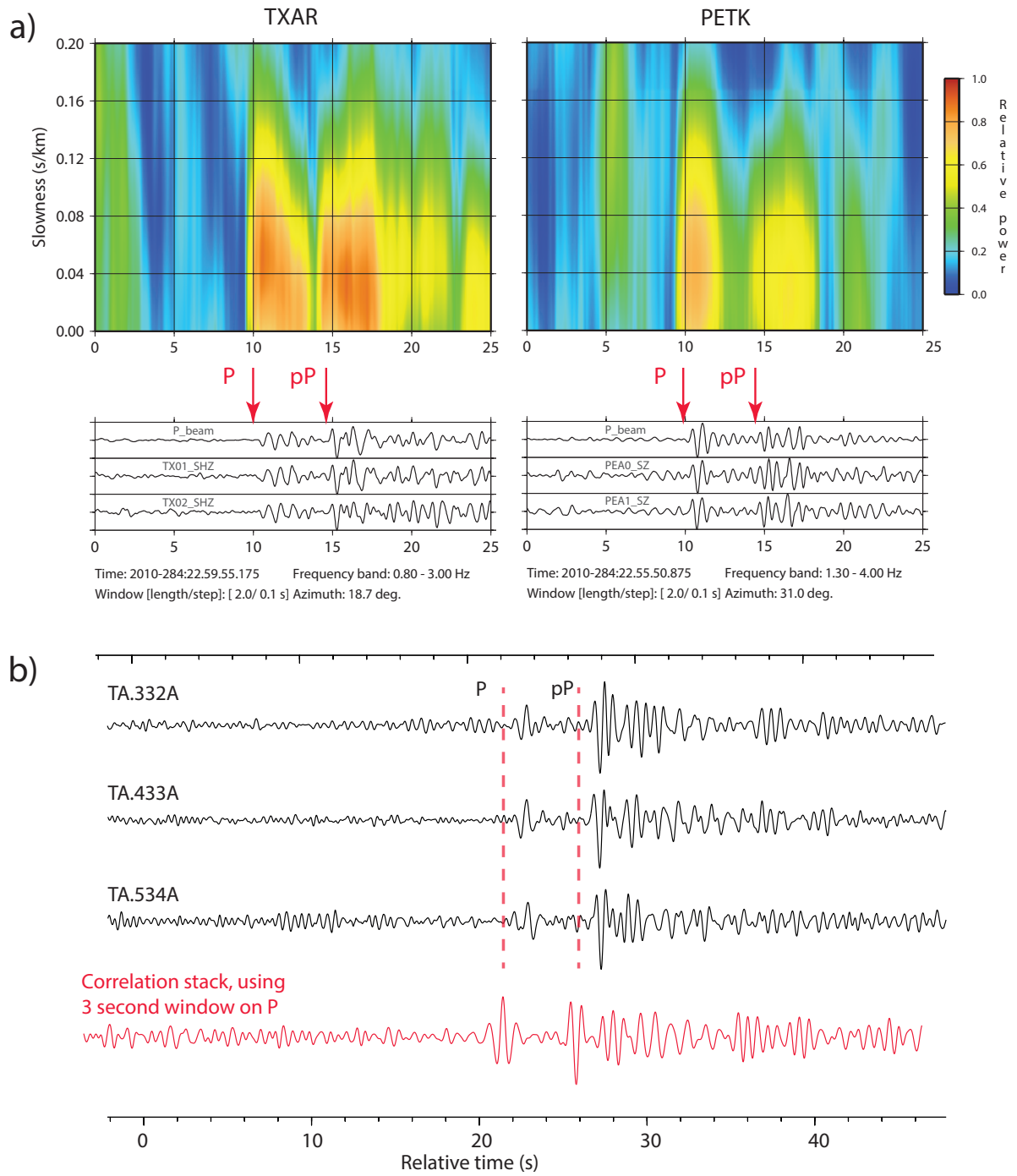


Figure 4. Figure 4 caption.

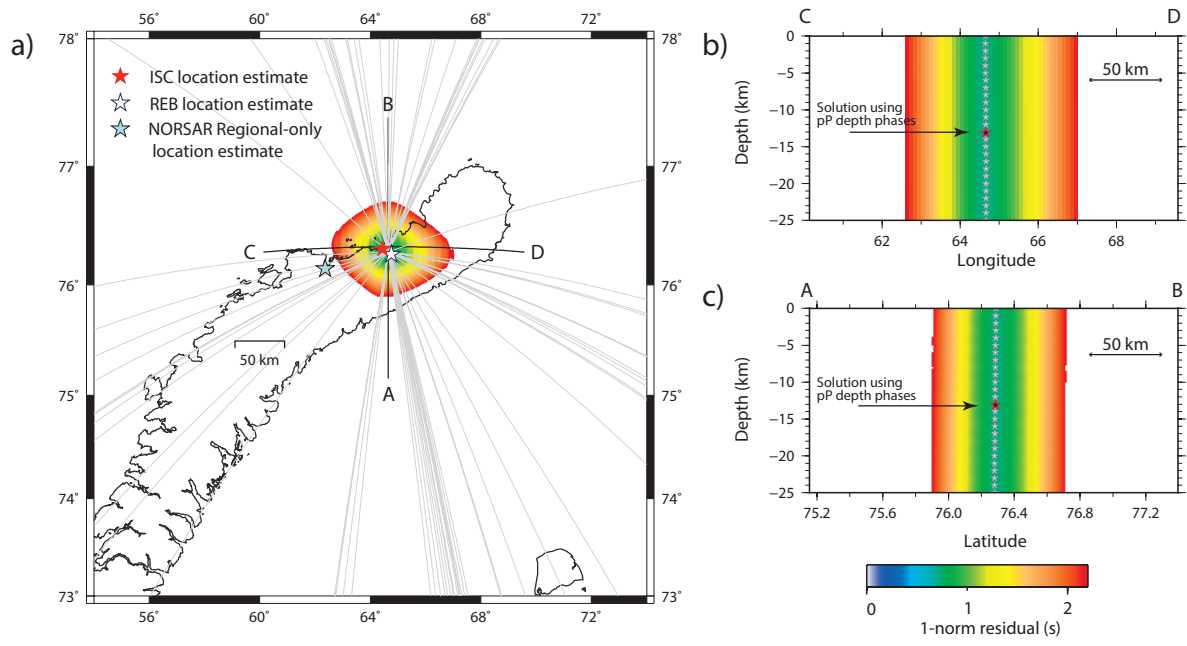


Figure 5. Figure 5 caption.



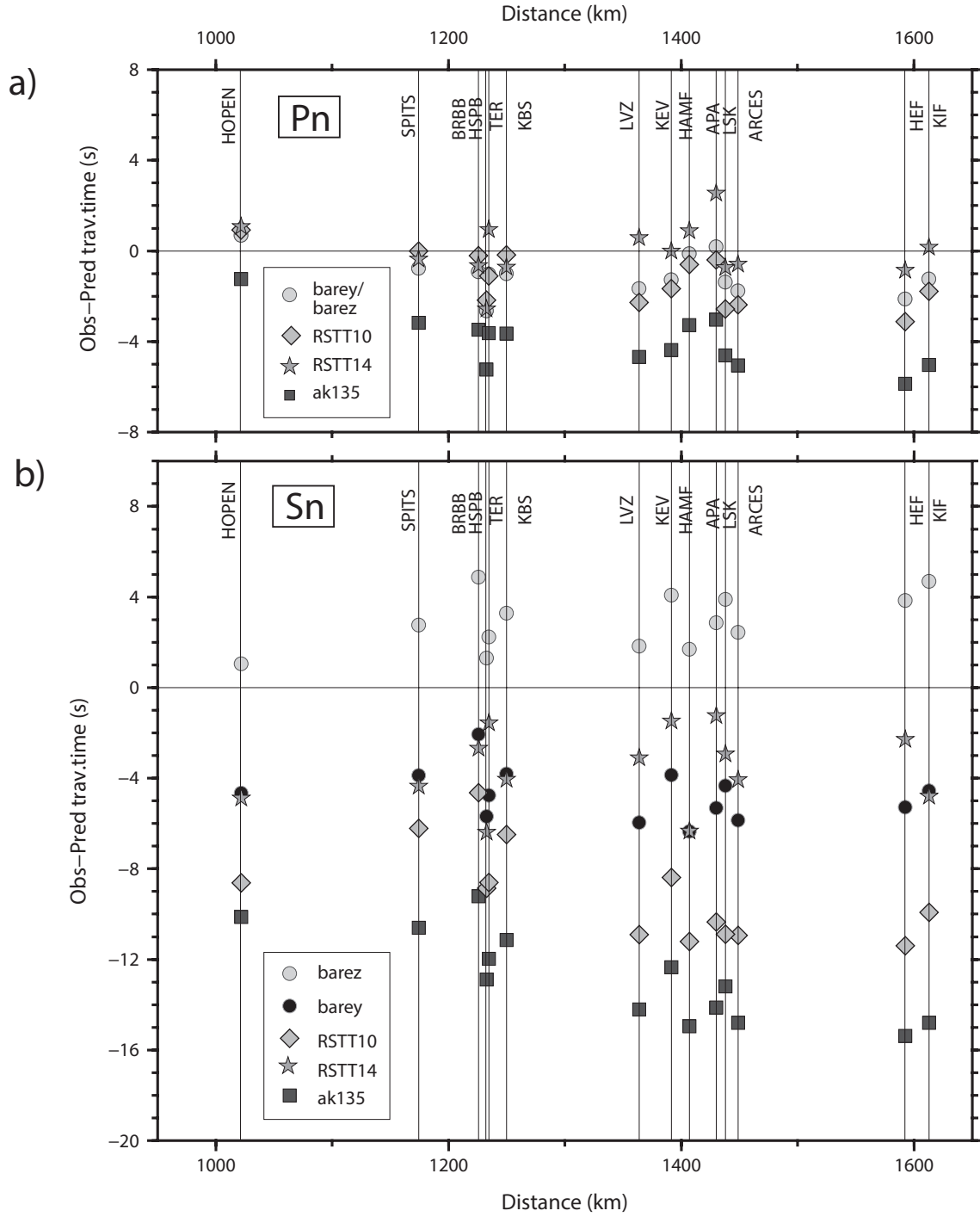


Figure 6. Figure 6 caption.

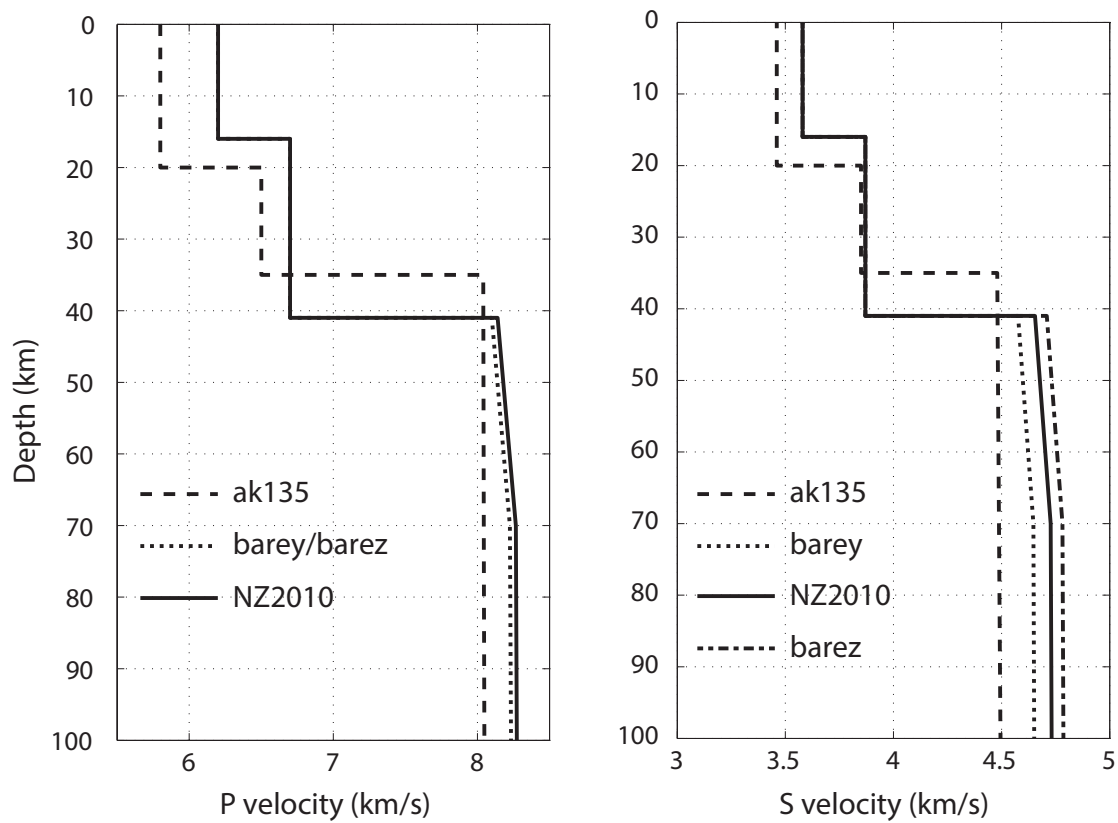


Figure 7. Figure 7 caption.

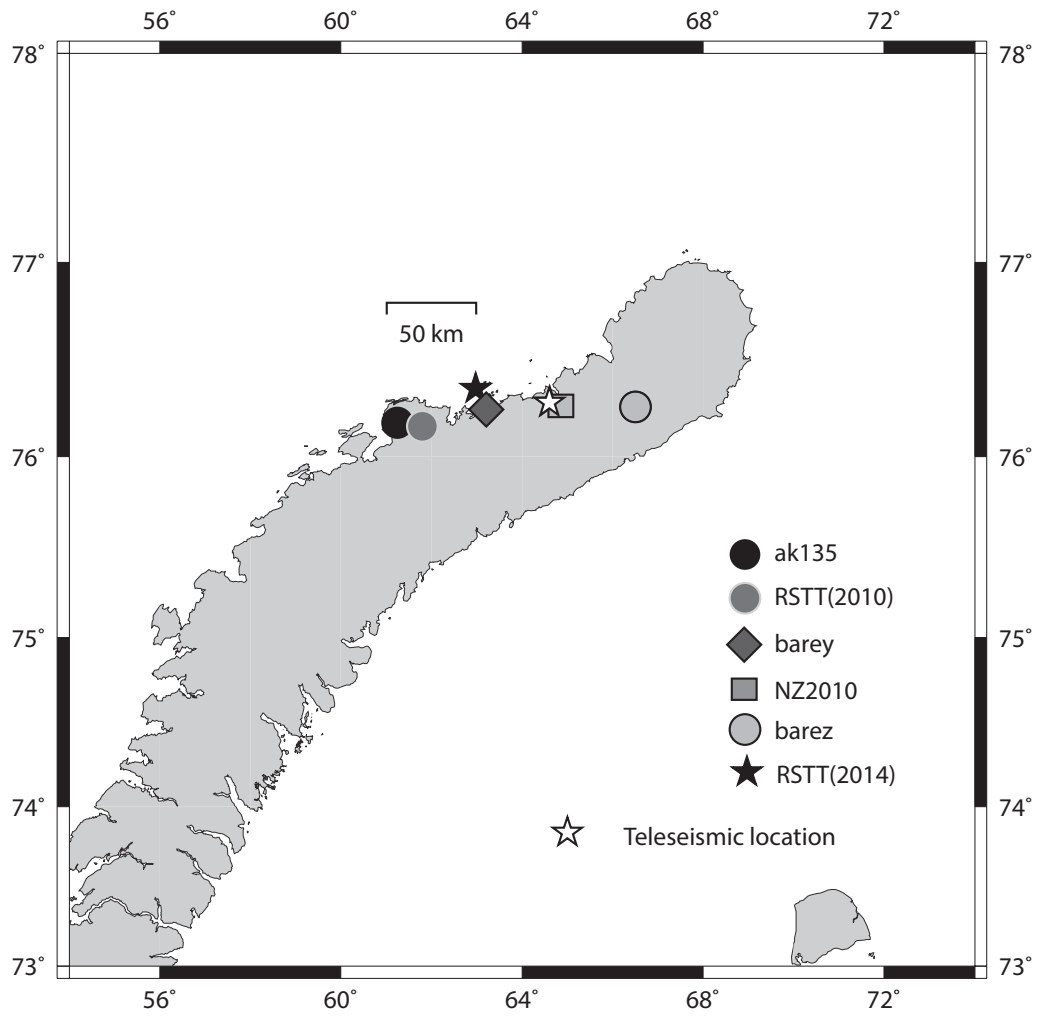


Figure 8. Figure 8 caption.

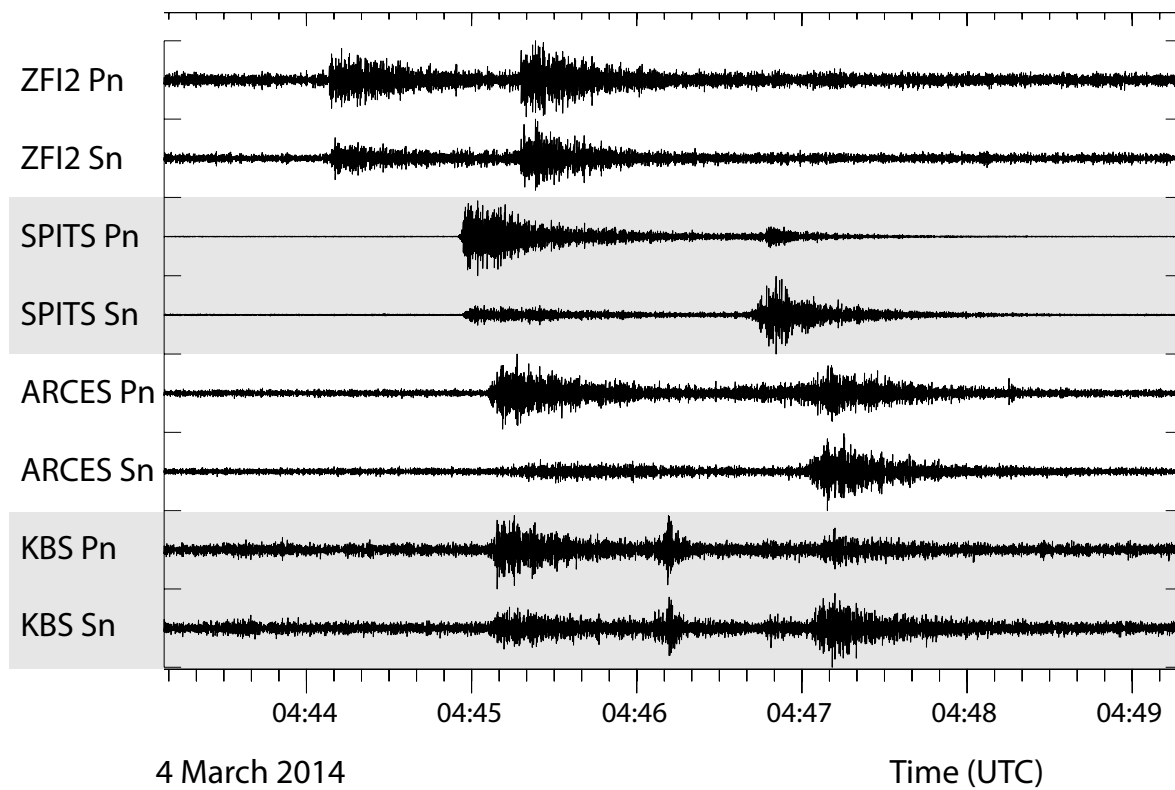


Figure 9. Figure 9 caption.

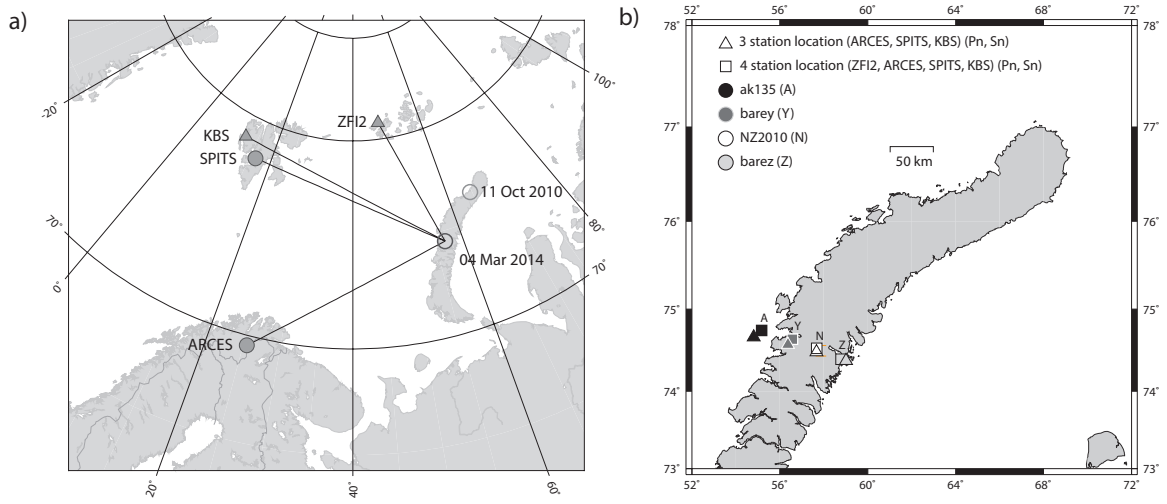


Figure 10. Figure 10 caption.